

## Constructing Functional Radiation-Resistant Thorium Clusters for Catalytic Redox Reactions

Qian Niu,<sup>||</sup> Tao-Yuan Yu,<sup>||</sup> Jing-Wen Shi, Qing Huang, Long-Zhang Dong, Fei Yu, Shun-Li Li, Jiang Liu,<sup>\*</sup> and Ya-Qian Lan<sup>\*</sup>



Cite This: <https://doi.org/10.1021/jacs.4c03126>



Read Online

ACCESS |



Metrics & More

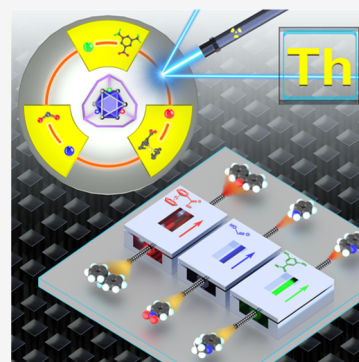


Article Recommendations



Supporting Information

**ABSTRACT:** When catalytic reactions are interfered with by radiation sources, thorium clusters are promising as potential catalysts due to their superior radiation resistance. However, there is currently very little research on the design synthesis and catalytic application of radiation-stable thorium clusters. In this work, we have elaborately engineered and fabricated three high-nuclear thorium cluster catalysts denoted as  $\text{Th}_{12}\text{L}_3\text{-MA}_{12}$ ,  $\text{Th}_{12}\text{L}_3\text{-MA}_6\text{-BF}_6$ , and  $\text{Th}_{12}\text{L}_3\text{-Fcc}_{12}$ , which did not undergo any significant alterations in their molecular structures and compositions after irradiation with 690 kGy  $\gamma$ -rays. We systematically investigated the photocatalytic/thermocatalytic properties of these radiation-resistant thorium clusters for the first time and found that  $\gamma$ -rays could not alter their catalytic activities. In addition, it was found that ligand engineering could modulate the catalytic activity of thorium clusters, thus expanding the range of catalytic applications of thorium clusters, including reduction reactions (nitroarene reduction) and some oxidation reactions (N-heterocyclic oxidative dehydrogenation and diphenylmethane oxidation). Meanwhile, all of these organic transformation reactions achieved a >80% conversion and nearly 100% product selectivity. Radiation experiments combined with DFT calculations showed that the synergistic catalysis of thorium-oxo core and ligands led to the generation of specific active species ( $\text{H}^+$ ,  $\text{O}_2^{\bullet-}$ , or  $t\text{BuO}/t\text{BuOO}^{\bullet}$ ) and activation of substrate molecules, thus achieving superior catalytic performance. This work is not only the first to develop radiation-resistant thorium cluster catalysts to perform efficient redox reactions but also provides design ideas for the construction of high-nuclearity thorium clusters under mild conditions.



## INTRODUCTION

Thorium, as the most plentiful naturally existing actinide, can be considered as a new frontier for nuclear energy.<sup>1</sup> In recent years, there has been a growing interest in the development and utilization of thorium-based materials, extending to areas such as adsorption, radiation visualization, and catalysis.<sup>2–5</sup> Notably, in the field of catalysis, the unique properties of thorium, with its large ionic size, high oxophilicity, and the presence of 5f and 6d orbitals, may allow it to show special activity in some chemical transformations.<sup>6–8</sup> Currently, many thorium-based complexes have been successfully applied in various organic catalytic transformations (hydroboration of amides, thioether oxidation, Cross–Tishchenko reactions, etc.), indicating the tremendous potential of thorium-based materials in the catalysis field.<sup>9–13</sup> However, the limited number of metal sites (generally no more than 6) and structures in most thorium-based complexes restricts their activity in certain catalytic reactions. Therefore, the design of novel thorium-based complexes, such as thorium clusters, is necessary to increase the number of metal sites and expand the structural diversity of thorium-based complexes, thereby enhancing their catalytic activity. In addition, introducing various functional ligands can also synergize with the metal to further enhance the catalytic activity and expand the range of

applications for thorium clusters. However, there are relatively few reports on thorium cluster catalysts, which is in part related to the difficulty in synthesis structures.<sup>14–16</sup> To date, the crystal structure of thorium clusters, particularly high-nuclear thorium clusters, is still relatively limited compared to other metal clusters (e.g., transition, main group, and lanthanide metals).<sup>17,18</sup> This is on account of the fact that  $\text{Th}^{4+}$  is susceptible to hydrolysis, which makes it more difficult to nucleate, commonly producing low-nucleated clusters or  $\text{ThO}_2$ .<sup>18–1923</sup> Therefore, the design and synthesis of stable highly nuclear thorium clusters remain a significant challenge.

Furthermore, the extremely difficult valence transition of thorium ions (typically +4 valence) and the fact that some catalytic reactions usually involve redox processes mean that thorium clusters may be “inert” to some catalytic reactions, which is one of the reasons why their catalytic properties have been less researched. Ligand engineering would be an effective

**Received:** March 3, 2024

**Revised:** July 2, 2024

**Accepted:** July 3, 2024



Scheme 1. Schematic Representation of the Cocatalysis of Radiation-Resistant Thorium-Oxo Core and Ligands to Modulate the Reaction Type

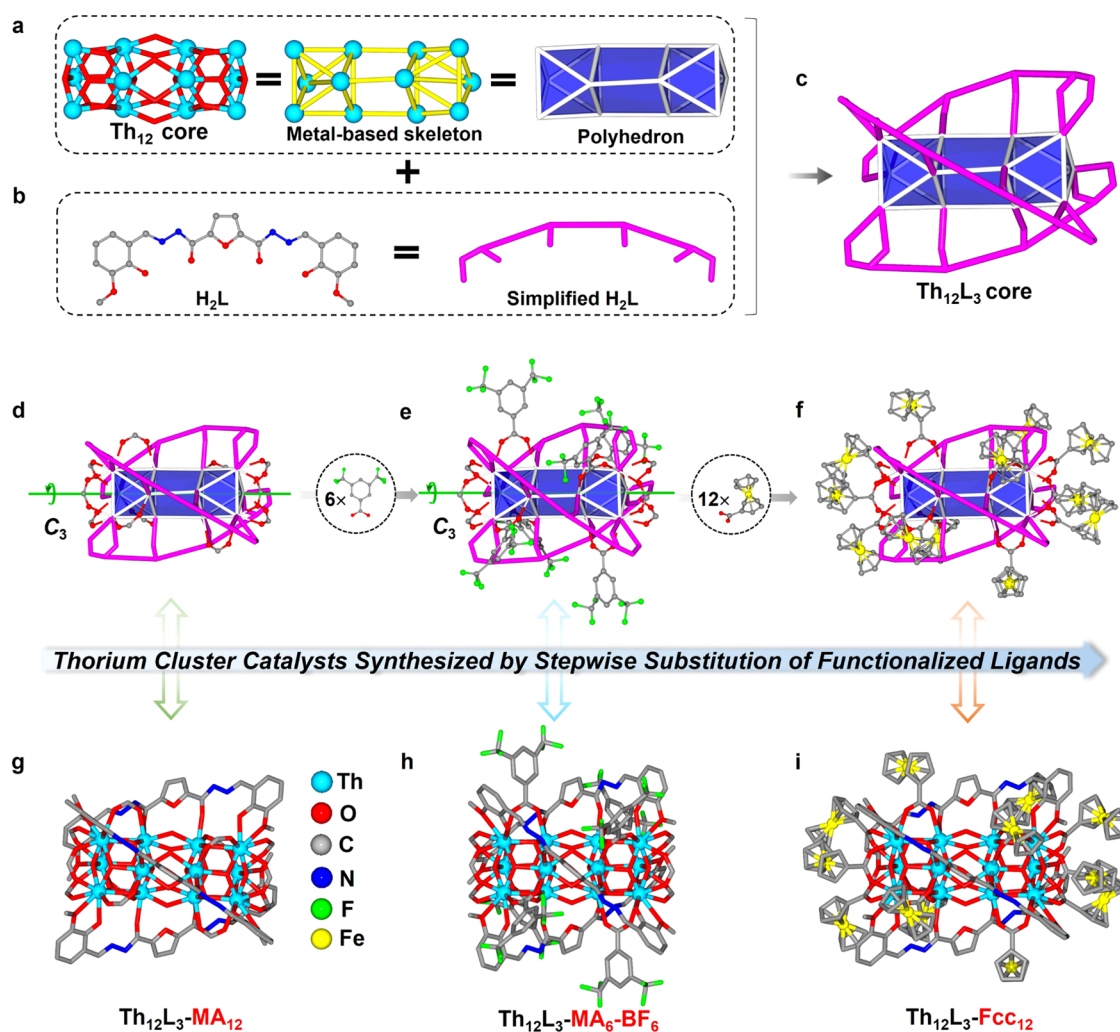
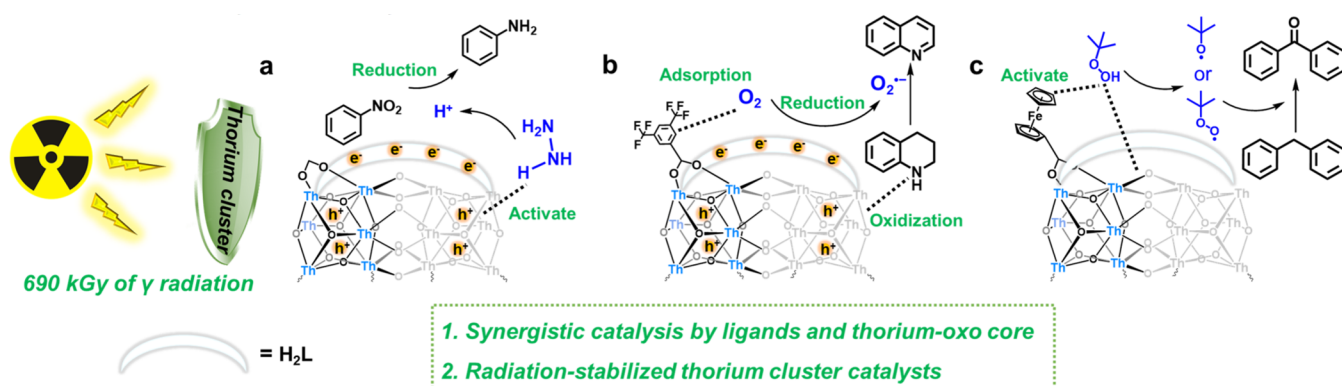


**Figure 1.** Crystal structure of four thorium clusters. (a)  $\text{Th}_{12}$  core and its simplified model. (b)  $\text{H}_2\text{L}$  and its simplified model. (c) Simplification of  $\text{Th}_{12}\text{L}_3$  core. The simplified structure of (d)  $\text{Th}_{12}\text{L}_3\text{-MA}_{12}$ , (e)  $\text{Th}_{12}\text{L}_3\text{-MA}_6\text{-BF}_6$ , and (f)  $\text{Th}_{12}\text{L}_3\text{-Fcc}_{12}$ . The molecular structure view of (g)  $\text{Th}_{12}\text{L}_3\text{-MA}_{12}$ , (h)  $\text{Th}_{12}\text{L}_3\text{-MA}_6\text{-BF}_6$ , and (i).  $\text{Th}_{12}\text{L}_3\text{-Fcc}_{12}$ . All hydrogen atoms are omitted for clarity.

strategy for solving the above issues.<sup>24</sup> On the one hand, ligand engineering can manipulate the synthesis and assembly process of thorium clusters, which is expected to synthesize high-nuclear thorium clusters, and, on the other hand, it can also modulate the electronic structure of thorium clusters to make them catalytically active and improve their stability, thus broadening the range of catalytic applications of thorium

clusters. It is worth noting that  $\text{Th}^{4+}$  has a high ionizing radiation scattering cross section and attenuation coefficient, which can endow thorium clusters with superior radioactivity stability than other materials.<sup>25–28</sup> This implies that thorium clusters can still maintain their catalytic activity and stability under potentially radioactive environments, which provides a potential application advantage to cope with possible radiation

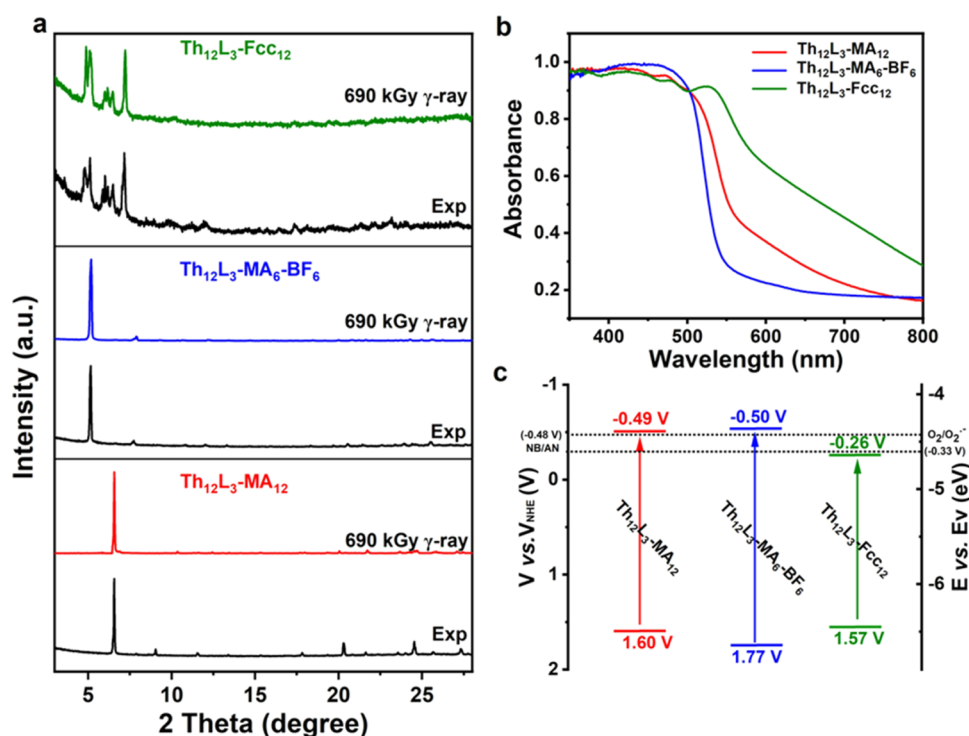


**Figure 2.** Characterization and optoelectronic properties of thorium clusters. (a) XRD spectra of three thorium cluster crystals before and after  $\gamma$ -ray irradiation. (b) UV–visible diffuse reflectance spectra for three thorium clusters. (c) Energy band diagrams of three thorium clusters.

78 sources in industrial catalysis processes; however, this has not  
79 been reported. Therefore, the design of highly nuclear thorium  
80 cluster catalysts with radioactive stability and the in-depth  
81 study of their catalytic properties can contribute to advancing  
82 the research of thorium cluster catalysts and realize their  
83 potential applications in specific catalytic fields.

84 Based on this, we have employed dual-ligand engineering to  
85 construct three highest-nuclearity thorium-oxo clusters to date  
86 under mild solvothermal conditions,  
87  $[\text{Th}_{12}\text{O}_8(\text{OH})_{14}(\text{HCOO})_{12}\text{L}_3]$  ( $\text{Th}_{12}\text{L}_3\text{-MA}_{12}$ ,  $\text{H}_2\text{L} = \text{N}^2, \text{N}^5$ -  
88 bis((*E*)-3-ethoxy-2-hydroxybenzylidene)-furan-2,5-dicarbohy-  
89 drazide,  $\text{MA} = \text{formic acid}$ ),  
90  $[\text{Th}_{12}\text{O}_8(\text{OH})_{14}(\text{BF})_6(\text{HCOO})_6\text{L}_3]$  ( $\text{Th}_{12}\text{L}_3\text{-MA}_6\text{-BF}_6$ ,  $\text{BF} =$   
91 3,5-bis(trifluoromethyl)benzoic acid), and  
92  $[\text{Th}_{12}\text{O}_8(\text{OH})_{14}(\text{Fcc})_{12}\text{L}_3]$  ( $\text{Th}_{12}\text{L}_3\text{-Fcc}_{12}$ ,  $\text{Fcc} = \text{ferrocenecar-}$   
93 boxylic acid). Among them, the bis(acylhydrazone) ligand  
94 ( $\text{H}_2\text{L}$ ) with powerful chelating ability can not only improve the  
95 stability of thorium clusters but also increase the nuclear  
96 number of thorium clusters.<sup>29,30</sup> The flexible  $\text{H}_2\text{L}$  ligands and  
97 the high coordination number of  $\text{Th}^{4+}$  leave a certain  
98 coordination space, which allows further introduction of  
99 secondary ligands (e.g., formic acid ligands with small steric  
100 hindrance, 3,5-bis(trifluoromethyl)benzoic acid with an  
101 electron-withdrawing group, and ferrocene with excellent  
102 redox ability). This not only further improves the stability  
103 but also alters the physicochemical properties and catalytic  
104 activity of the thorium clusters, which allows these clusters to  
105 be exploited as a model system to investigate the effects of  
106 “dual-ligand engineering”. Furthermore, the molecular struc-  
107 ture and composition of these thorium clusters did not change  
108 significantly after irradiation with 690 kGy  $\gamma$ -rays (with a dose  
109 rate of  $15.5 \text{ kGy h}^{-1}$ ). Therefore, we applied these function-  
110 alized irradiation-resistant thorium clusters to reduction  
111 reaction (photocatalytic reduction of nitrobenzene) and

some oxidation reactions (photocatalytic N-heterocyclic  
oxidative dehydrogenation and thermal catalytic oxidation of  
diphenylmethane). Their catalytic activities were comparable  
to those before  $\gamma$ -ray irradiation, which means that these  
thorium clusters will be promising for catalysts that need to be  
exposed to ionizing radiation conditions in the future. In these  
reactions, the catalytic activity of irradiated crystals varies for  
each, which is closely related to the incorporation of the  
second ligand, suggesting that the ligand engineering strategy is  
indeed an attractive way to tailor the catalytic properties.  
Furthermore, experimental and theoretical calculations dem-  
onstrate that the thorium-oxo core and the ligand complement  
each other in these reactions to achieve efficient transformation  
of the substrate molecules (Scheme 1). To the best of our  
knowledge, this work not only develops radiation-resistant  
thorium cluster catalysts to execute redox reactions for the first  
time but also provides a new strategy for building high-nuclear  
thorium clusters under mild conditions.

## RESULTS AND DISCUSSION

**Synthesis and Structure of Thorium Clusters.** The  
structure of  $\text{Th}_{12}\text{L}_3\text{-MA}_{12}$ ,  $\text{Th}_{12}\text{L}_3\text{-MA}_6\text{-BF}_6$ , and  $\text{Th}_{12}\text{L}_3\text{-Fcc}_{12}$   
was established by single-crystal X-ray diffraction (SCXRD).  
As shown in Figure 1a, these thorium clusters comprise the  
similar and rare  $\{\text{Th}_{12}\}$  core, which is composed of two  
identical  $\{\text{Th}_6\}$  building blocks. The  $\{\text{Th}_6\}$  is composed of  
three nine-coordinated and three eight-coordinated Th atoms,  
bridged by four  $\mu_3\text{-OH}$  and four  $\mu_3\text{-O}$  groups. Each  $\{\text{Th}_6\}$   
forms an octahedron, and the middle of the two octahedra is  
connected by bridging oxygen to form a trigonal prism.  
Further, these thorium clusters also possess the same  $\text{Th}_{12}\text{L}_3$   
core, which is three  $\text{H}_2\text{L}$  making two  $\{\text{Th}_6\}$  bridged by six  $\mu_2\text{-}$   
OH groups (Figure 1c). Due to the high coordination number  
of  $\text{Th}^{4+}$ , the secondary ligand can be modified to the  $\text{Th}_{12}\text{L}_3$



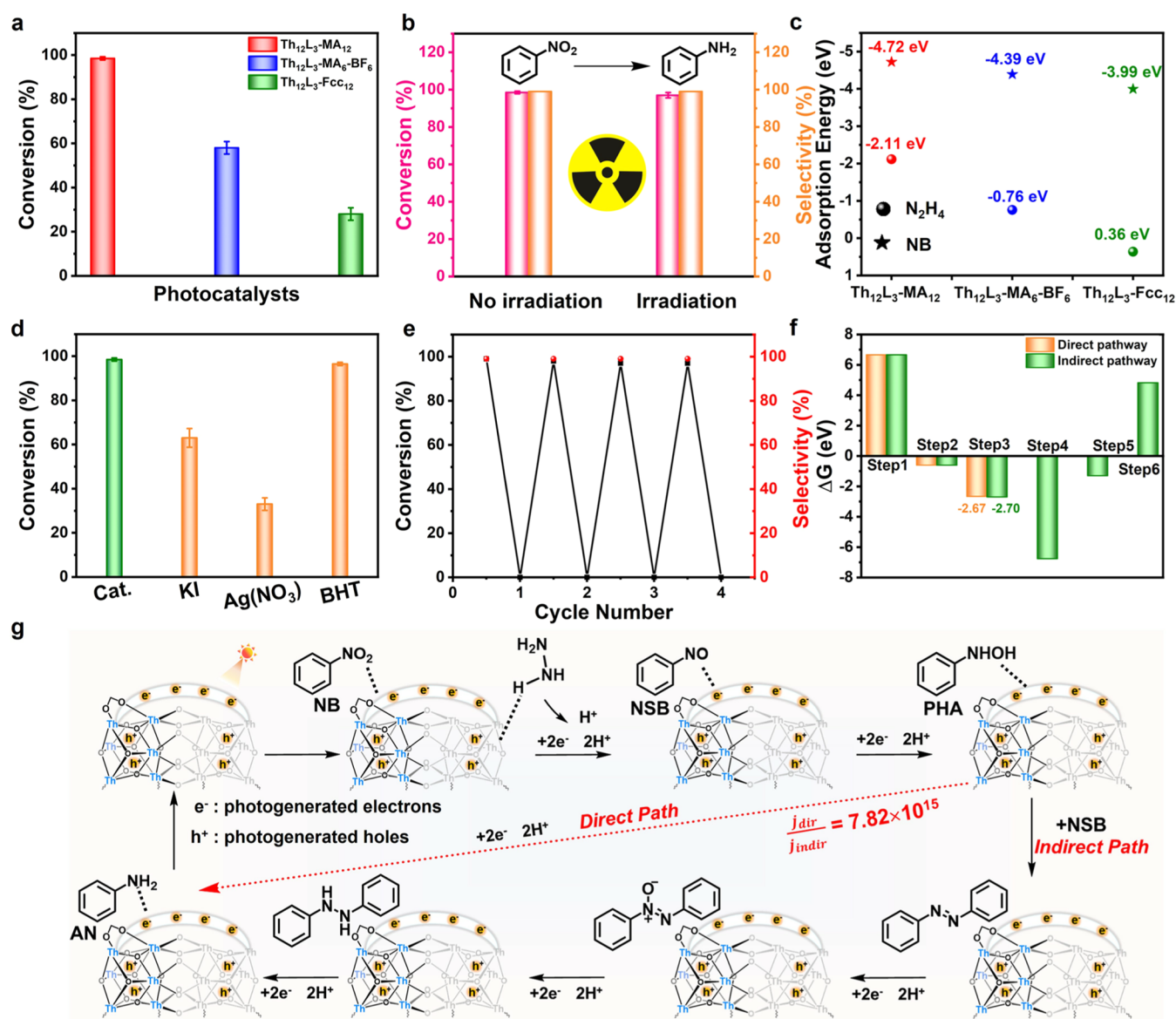


**Figure 3.** Photocatalytic reduction of nitroarenes. (a) Comparison of the catalytic properties of three thorium clusters irradiated with  $\gamma$ -rays. (b) Compared catalytic activity of  $\text{Th}_{12}\text{L}_3\text{-MA}_{12}$  before and after  $\gamma$ -irradiation. (c) The calculated adsorption energies of  $\text{N}_2\text{H}_4$  and NB on these three thorium clusters. (d) Some comparative tests added the corresponding sacrificial reagents. (e) The conversion and selectivity of photocatalytic reduction of nitroarenes with  $\text{Th}_{12}\text{L}_3\text{-MA}_{12}$  in 4 repeating cycles. (f) Calculation of Gibbs free-energy distributions for two possible pathways of nitrobenzene reduction. (g) Photocatalytic nitrobenzene reduction mechanism (In the presence of light, the semiconductor-like material absorbs the light and produces electron-hole pairs).

core. When the MA ligand is introduced, orange  $\text{Th}_{12}\text{L}_3\text{-MA}_{12}$  crystals can be obtained, which crystallize in the trigonal space group  $R\bar{3}c$ . Its structure consists of  $\text{Th}_{12}\text{L}_3$  core and 12 MA ligands, and its asymmetric unit involves four Th atoms (nine-coordinated Th1 and Th3, as well as eight-coordinated Th2 and Th4), five  $\mu_2$ -OH, one  $\text{H}_2\text{L}$ , five  $\mu_3$ -O/OH, and four MA ligands (Figure S4a). Three MA ligands chelate three Th1/Th3 atoms at one  $\mu_3$ -O capped face. At the same time, three Th2/Th4 atoms also form a triangular face, and the other MA ligands bridge the Th1 and Th2 atoms or Th3 and Th4 atoms (Figure S4c). Interestingly,  $\text{Th}_{12}\text{L}_3\text{-MA}_{12}$  has exactly a  $C_3$  symmetry axis passing through the center of the two faces (Figure S4d). When the positions of six MA were occupied by BF, many yellow crystals of  $\text{Th}_{12}\text{L}_3\text{-MA}_6\text{-BF}_6$  are formed. SCXRD analysis indicates that it has the same space group and

crystallographic symmetry  $C_3$  axis as  $\text{Th}_{12}\text{L}_3\text{-MA}_{12}$  (Figure S5d). The only difference is that it has two MA and two BF in the asymmetric unit instead of four MA ligands, which leads to BF ligands bridging the Th1 and Th2 atoms or Th3 and Th4 atoms (Figure S5a). Further, when the coordination positions of MA and BF were encroached by 12 Fcc ligands, orange crystals of  $\text{Th}_{12}\text{L}_3\text{-Fcc}_{12}$  with high crystallinity were formed. SCXRD analysis indicates that it crystallizes in a triclinic crystal system with the space group  $P\bar{1}$ . As shown in Figure S6a, its asymmetric unit consists of the  $\text{Th}_{12}\text{L}_3$  core decorated by 12 Fcc ligands. It is remarkable that its 12 Th atoms are completely independent, where Th4–Th9 are eight-coordinated, and the rest are nine-coordinated (Figure S6b). Apparently, the crystal structures of these thorium clusters can not only maintain almost identical  $\text{Th}_{12}\text{L}_3$  core but also the coordination patterns of their secondary ligands are also the



same through ligand gradual substitution strategy. This allows them to be used as a model system to investigate the catalytic performance differences, which is still relatively rare.

**Characterization and Optoelectronic Properties of Thorium Clusters.** The powder X-ray diffraction (PXRD) patterns of as-synthesized thorium clusters were in good accordance with the simulation results of crystallographic data, which substantiated that they had excellent crystallinity. The chemistry stability of these thorium clusters was determined by dipping crystals into aqueous solutions with different pH values (Figures S7–S9 and Table S2). Among these thorium clusters,  $\text{Th}_{12}\text{L}_3\text{-MA}_6\text{-BF}_6$  has relatively high chemical stability between pH 1 and 13, which is inextricably associated with the hydrophobicity of 3,5-bis(trifluoromethyl)benzoic acid. In addition, the thermogravimetric analysis (TGA) results suggested that these thorium clusters can remain thermodynamically stable before 250 °C (Figure S10). Remarkably, when irradiated with  $\gamma$ -rays up to 690 kGy, the PXRD and IR results showed that these thorium clusters still maintain their original structures (Figures 2a and S11). This means that these thorium cluster crystals can be used in some catalytic reactions that require exposure to radiation. Due to the high radiation resistance of thorium, it can tolerate a further amount of irradiation, which will be further designed according to the actual application scenarios.

Next, solid-state ultraviolet–visible (UV–vis) absorption was undertaken to assess the light absorption capacity of these thorium clusters. Compared with  $\text{H}_2\text{L}$  ligand, the strong visible light absorption of  $\text{Th}_{12}\text{L}_3\text{-MA}_{12}$ ,  $\text{Th}_{12}\text{L}_3\text{-MA}_6\text{-BF}_6$ , and  $\text{Th}_{12}\text{L}_3\text{-Fcc}_{12}$  extends to ~550, 520, and 600 nm, respectively (Figures 2b and S12). The band-gap energies of  $\text{Th}_{12}\text{L}_3\text{-MA}_{12}$ ,  $\text{Th}_{12}\text{L}_3\text{-MA}_6\text{-BF}_6$ , and  $\text{Th}_{12}\text{L}_3\text{-Fcc}_{12}$  were 2.09, 2.27, and 1.83 eV, respectively, suggesting their semiconductor-like characteristics (Figure S13). Subsequently, the HOMO–LUMO energy levels of these thorium clusters were estimated using ultraviolet photoelectron spectroscopy (UPS) technology. The highest occupied molecular orbital (HOMO) positions of  $\text{Th}_{12}\text{L}_3\text{-MA}_{12}$ ,  $\text{Th}_{12}\text{L}_3\text{-MA}_6\text{-BF}_6$ , and  $\text{Th}_{12}\text{L}_3\text{-Fcc}_{12}$  were estimated to be 1.60, 1.77, and 1.57 V, and their corresponding lowest unoccupied molecular orbital (LUMO) positions were –0.49, –0.5, and –0.26 V (Figures 2c and S14). Photocurrent response tests and electrochemical impedance spectroscopy (EIS) were also performed to evaluate the separation efficiency of photogenerated electrons ( $\text{e}^-$ ) and holes ( $\text{h}^+$ ) of these thorium clusters. The enhanced photocurrent of the  $\text{Th}_{12}\text{L}_3\text{-MA}_6\text{-BF}_6$  and  $\text{Th}_{12}\text{L}_3\text{-Fcc}_{12}$  compared to that of  $\text{Th}_{12}\text{L}_3\text{-MA}_{12}$  indicated an increase in charge mobility, which is consistent with the EIS results (Figures S15 and S16). Additionally, photoluminescence (PL) and time-resolved fluorescence decay techniques were conducted to investigate the charge separation behaviors. Compared to  $\text{Th}_{12}\text{L}_3\text{-MA}_{12}$ , the PL intensity of  $\text{Th}_{12}\text{L}_3\text{-MA}_6\text{-BF}_6$  and  $\text{Th}_{12}\text{L}_3\text{-Fcc}_{12}$  was significantly quenched (Figure S17). Also, the fluorescence lifetimes of  $\text{Th}_{12}\text{L}_3\text{-MA}_6\text{-BF}_6$  (2.12 ns) and  $\text{Th}_{12}\text{L}_3\text{-Fcc}_{12}$  (2.45 ns) were also longer than that of  $\text{Th}_{12}\text{L}_3\text{-MA}_{12}$  (2.00 ns) (Table S5). This indicates that the  $\text{e}^-$ – $\text{h}^+$  pair recombination becomes lower, and the separation efficiency is higher for  $\text{Th}_{12}\text{L}_3\text{-MA}_6\text{-BF}_6$  and  $\text{Th}_{12}\text{L}_3\text{-Fcc}_{12}$ . These results suggest that the dual-ligand engineering strategy, while maintaining almost identical structures, surprisingly can also modulate the stability and structural properties of thorium clusters (light absorption, energy band structure, and photogenerated  $\text{e}^-$ – $\text{h}^+$  separation

ability, etc.), which may affect their catalytic ability in different reactions.

**Photocatalytic Reduction of Nitroarenes.** The reduction of nitroarenes to the corresponding amines is a pivotal process in the fine and bulk chemical industries.<sup>31–33</sup> However, the reduction of nitroarenes also yields byproducts (azo and azoxy). Therefore, it is of great significance to design catalysts for highly selective reduction of nitroarenes driven by light. In view of the remarkable light-absorbing ability, tunable energy band structure, and high radiation stability of thorium clusters, we envisioned to utilize thorium clusters after 690 kGy  $\gamma$  irradiation as catalysts to evaluate their photocatalytic reduction activity of nitroarenes using nitrobenzene (NB) as a substrate and hydrazine hydrate ( $\text{N}_2\text{H}_4\text{-H}_2\text{O}$ ) as a hydrogen donor. The results showed that the photocatalytic activity of  $\text{Th}_{12}\text{L}_3\text{-MA}_{12}$  was higher, with a conversion of 98%, than that of  $\text{Th}_{12}\text{L}_3\text{-MA}_6\text{-BF}_6$  (60%) and  $\text{Th}_{12}\text{L}_3\text{-Fcc}_{12}$  (26%), which was comparable to that of the unirradiated catalytic activity. It is further demonstrated that  $\gamma$  irradiation does not change the catalytic activity of thorium clusters (Figure 3a,b). To explain the differences between these thorium clusters, the adsorption energy of  $\text{N}_2\text{H}_4$  on these three thorium clusters was calculated first. Figure 3c shows that the adsorption energies of  $\text{N}_2\text{H}_4$  on these thorium clusters increased in the order of  $\text{Th}_{12}\text{L}_3\text{-MA}_{12}$  (–2.11 eV) <  $\text{Th}_{12}\text{L}_3\text{-MA}_6\text{-BF}_6$  (–0.76 eV) <  $\text{Th}_{12}\text{L}_3\text{-Fcc}_{12}$  (0.36 eV), which implied that  $\text{Th}_{12}\text{L}_3\text{-MA}_{12}$  is more capable of adsorption and activation of  $\text{N}_2\text{H}_4$ . Similarly, the adsorption energy of nitrobenzene followed the above pattern, leading to a decreasing catalytic performance in the order of  $\text{Th}_{12}\text{L}_3\text{-MA}_{12}$  >  $\text{Th}_{12}\text{L}_3\text{-MA}_6\text{-BF}_6$  >  $\text{Th}_{12}\text{L}_3\text{-Fcc}_{12}$ .

Next, a series of comparative experiments (metal salts, ligands, and  $\text{Th}_6$ ) were performed to demonstrate the importance of high-nuclear thorium clusters in photocatalysis (Table 1). Undoubtedly, these catalysts exhibited relatively low catalytic activity, much lower than the performance of  $\text{Th}_{12}\text{L}_3\text{-MA}_{12}$ , which further demonstrated the catalytic advantage of synthesizing high-nuclear thorium clusters and the synergistic effects between the thorium-oxo core and ligands in the structure. In addition, secondary catalytic experiments were performed on the filtrate after the reaction, and in this experiment, little significant conversion was observed, which further excludes the influence of thorium cluster decomposition products on the reaction (Table S4). Quenching experiments were subsequently performed to demonstrate the role of active species in the reaction process (Figure 3d and Table S6). The results suggest that photogenerated electrons and holes are indispensable. Furthermore, the active hydrogen species in this reaction should be  $\text{H}^+$ , not  $\text{H}^\bullet$  radicals. In addition, XPS, XRD, and FTIR analysis before and after the reaction confirmed the preservation of the structural features of  $\text{Th}_{12}\text{L}_3\text{-MA}_{12}$  (Figures S19–S21). At the same time, the ICP results showed that only 0.005% of  $\text{Th}^{4+}$  remained in the filtrate after the reaction (Table S3). The results of the cycling experiments also indicated that the loss of catalytic activity was very marginal even after the fourth cycle (Figure 3e), which further demonstrated the advantages of thorium clusters as heterogeneous catalysts over homogeneous ones ( $\text{Th}(\text{NO}_3)_4$ ). As expected,  $\text{Th}_{12}\text{L}_3\text{-MA}_{12}$  can also effectively reduce a wide variety of substrates with high selectivity (Figure S22).

Subsequently, the pathways of nitrobenzene reduction are examined in depth. Two pathways are known: one is through the nitrosobenzene (NSB) and phenylhydroxylamine (PHA) intermediates to produce aniline (AN) (direct pathway); the

**Table 1. A Series of Comparative Experiments on These Three Reactions**

entry	photocatalyst	conv. (%) <sup>d</sup>	sele. (%) <sup>d</sup>
1	Th <sub>12</sub> L <sub>3</sub> -MA <sub>12</sub>	98.0	99
2 <sup>a</sup>	Th <sub>12</sub> L <sub>3</sub> -MA <sub>6</sub> -BF <sub>6</sub>	62.0	99
3 <sup>a</sup>	Th <sub>12</sub> L <sub>3</sub> -Fcc <sub>12</sub>	26.0	99
4 <sup>a</sup>	Th <sub>6</sub>	28.4	99
5 <sup>a</sup>	H <sub>2</sub> L	33.0	99
6 <sup>a</sup>	Th(NO <sub>3</sub> ) <sub>4</sub>	55.0	99
7 <sup>b</sup>	Th <sub>12</sub> L <sub>3</sub> -MA <sub>12</sub>	63.0	99
8 <sup>b</sup>	Th <sub>12</sub> L <sub>3</sub> -MA <sub>6</sub> -BF <sub>6</sub>	99.0	99
9 <sup>b</sup>	Th <sub>12</sub> L <sub>3</sub> -Fcc <sub>12</sub>	39.0	99
10 <sup>b</sup>	Th <sub>6</sub>	38.8	99
11 <sup>b</sup>	H <sub>2</sub> L+BF	9.0	99
12 <sup>b</sup>	Th(NO <sub>3</sub> ) <sub>4</sub>	29.9	99
13 <sup>c</sup>	Th <sub>12</sub> L <sub>3</sub> -MA <sub>12</sub>	22.0	99
14 <sup>c</sup>	Th <sub>12</sub> L <sub>3</sub> -MA <sub>6</sub> -BF <sub>6</sub>	29.0	99
15 <sup>c</sup>	Th <sub>12</sub> L <sub>3</sub> -Fcc <sub>12</sub>	85.0	99
16 <sup>c</sup>	Th <sub>6</sub>	25.2	99
17 <sup>c</sup>	Fcc+H <sub>2</sub> L	59.0	99
18 <sup>c</sup>	Th(NO <sub>3</sub> ) <sub>4</sub>	45.0	99

<sup>a</sup>NB (0.05 mmol), catalyst 10 mg, isopropanol 1 mL, N<sub>2</sub>H<sub>4</sub>·H<sub>2</sub>O (2 mmol), 30 °C, 6 h, full spectrum irradiation. <sup>b</sup>1,2,3,4-THQ (0.05 mmol), catalysts 20 mg, solvent 1 mL of acetonitrile, reaction time 20 h under an O<sub>2</sub> atmosphere, in full spectrum irradiation (*T* = 25 °C). <sup>c</sup>DPM (0.05 mmol), catalysts 10 mg, solvent 1 mL of acetonitrile, reaction time 14 h, TBHP (70% w/w.), *T* = 80 °C. <sup>d</sup>Determined by GC.

other is through azoxybenzene and azobenzene (indirect pathway) (Figure S36). To specify the reaction pathways, Gibbs free-energy calculations were first performed, which showed that the energies required for the formation of C<sub>6</sub>H<sub>7</sub>N\* (−2.67 eV) and C<sub>12</sub>H<sub>10</sub>N<sub>2</sub>O\* (−2.70 eV) are close to each other, implying that the reaction pathway cannot be judged from a thermodynamic point of view only (Figure 3f). Subsequently, microkinetic simulations were carried out via a microkinetic model, which showed that the direct pathway occurs 15 orders of magnitude more frequently than the indirect pathway, making it almost impossible to take the indirect route (Figure S36). Further, to clarify the active site on Th<sub>12</sub>L<sub>3</sub>-MA<sub>12</sub>, the adsorption energy of N<sub>2</sub>H<sub>4</sub> at different positions (H<sub>2</sub>L and thorium-oxo core) was calculated. The adsorption energy on the thorium-oxo core is much lower than that on H<sub>2</sub>L (−2.11 vs 0.77 eV), suggesting that the thorium-oxo core should be the main site of N<sub>2</sub>H<sub>4</sub> adsorption and activation (Figure S38). Based on the above research and literature reports,<sup>34</sup> the possible mechanism is proposed in Figure 3g. Th<sub>12</sub>L<sub>3</sub>-MA<sub>12</sub> as semiconductor-like materials can be excited under light irradiation to produce e<sup>−</sup>–h<sup>+</sup> pairs. The photogenerated electrons are smoothly transferred to the H<sub>2</sub>L ligand, and N<sub>2</sub>H<sub>4</sub> is mainly activated by photogenerated holes on the thorium–oxygen core, accompanied by the generation of H<sup>+</sup>. Adjacent to the H<sub>2</sub>L ligand, the generated H<sup>+</sup> and photogenerated electrons cause a 6-electron and proton reduction of nitrobenzene to produce aniline.

**Photocatalytic Oxo-Dehydrogenation of N-Heterocycles.** Catalytic oxidative dehydrogenation (ODH) of saturated N-heterocyclic aromatics is one of the most commonly used methods for the synthesis of N-heterocycles, which are key intermediates for a range of drugs and biologically active molecules. Compared with conventional thermal catalysis, light-driven ODH reactions are quite

attractive.<sup>35–37</sup> However, only a few photocatalysts are currently used for ODH reactions. Thus, the development of efficient photocatalysts is imminent. Due to the tunable energy band structure of thorium clusters, they can not only satisfy the energy band of reduction reactions but also are expected to be used for ODH reactions. Therefore, we investigated for the first time the ODH reactivity of these thorium clusters after  $\gamma$ -irradiation using 1,2,3,4-tetrahydroquinoline (1,2,3,4-THQ) as a model substrate. Under the O<sub>2</sub> atmosphere, Th<sub>12</sub>L<sub>3</sub>-MA<sub>6</sub>-BF<sub>6</sub> showed a high reactivity with up to 99% quinoline selectivity, while Th<sub>12</sub>L<sub>3</sub>-MA<sub>12</sub> and Th<sub>12</sub>L<sub>3</sub>-Fcc<sub>12</sub> displayed poor photocatalytic activity (61 and 40%) (Figure 4a). This may be attributed to the stronger adsorption and activation of O<sub>2</sub> by 3,5-bis(trifluoromethyl)benzoic acid modification. Similarly, Th<sub>12</sub>L<sub>3</sub>-MA<sub>6</sub>-BF<sub>6</sub> without ionizing irradiation had also high photocatalytic activity (Figure 4b). Subsequently, a series of control experiments showed little quinoline production in the absence of a photocatalyst or light irradiation (Table S8). Meanwhile, Th<sub>12</sub>L<sub>3</sub>-MA<sub>6</sub>-BF<sub>6</sub> exhibits higher photocatalytic activity compared to the ligands, metal salts, and Th<sub>6</sub>, which is closely correlated with the increased number of metal sites and the synergistic effect between the ligands and the thorium-oxo core (Table 1). In addition, the results of secondary catalysis experiments performed on the reaction filtrate further indicate that thorium clusters play a dominant role in the catalytic reaction rather than its decomposition products (Table S4).

It is remarkable that the conversion of 1,2,3,4-THQ in the air can also reach very high (98%) for Th<sub>12</sub>L<sub>3</sub>-MA<sub>6</sub>-BF<sub>6</sub>. However, when the reaction atmosphere became inert gas (N<sub>2</sub>), the activity was poor (Table S8, entry 4). So, O<sub>2</sub> is very important in this reaction. The role of O<sub>2</sub> was further illustrated by EPR experiments using 5,5-dimethyl-1-pyrroline N-oxide (DMPO) as a radical spin trapping agent. Under light irradiation, the strong characteristic peaks of DMPO–O<sub>2</sub>• were clearly detected for Th<sub>12</sub>L<sub>3</sub>-MA<sub>6</sub>-BF<sub>6</sub>, while no radical signal was observed from EPR under dark conditions (Figure 4c). Moreover, reactive species quenching experiments were also performed to verify that O<sub>2</sub>• was the dominant reactive species in the ODH reaction (Figure 4d). The crystallinity and structural integrity of Th<sub>12</sub>L<sub>3</sub>-MA<sub>6</sub>-BF<sub>6</sub> were retained after the reaction, as confirmed by PXRD, FTIR, and XPS characterizations (Figures S23–S25). Meanwhile, ICP results showed that the residual of Th<sup>4+</sup> in the filtrate after the reaction was 0.0025% (Table S3). Subsequently, the recycling tests confirmed that the Th<sub>12</sub>L<sub>3</sub>-MA<sub>6</sub>-BF<sub>6</sub> could retain the catalytic activity and selectivity after four cycles (Figure 4e). Substrate broadening experiments showed that derivatives of 1,2,3,4-THQ (–F, –Cl, –Br, –Me, –OMe) could also be efficiently oxidized. Moreover, indoline and even indoline substituent (–Me) could be successfully converted to the corresponding indoles (Figure S26).

Density-functional theory (DFT) calculations were carried out to further explain the differences between the properties of these thorium clusters, and the results showed that the adsorption energy of O<sub>2</sub> on Th<sub>12</sub>L<sub>3</sub>-MA<sub>6</sub>-BF<sub>6</sub> is lower than that of the other thorium clusters, which proves that it is more capable of adsorption and activation of O<sub>2</sub> (Figure 4f). In addition, DFT calculations show that there is a significant charge density difference between these thorium clusters in the presence of O<sub>2</sub>. The Bader charge of oxygen molecules on Th<sub>12</sub>L<sub>3</sub>-MA<sub>6</sub>-BF<sub>6</sub> is −0.083 e, which is smaller to that of the other thorium clusters, suggesting that more electrons are

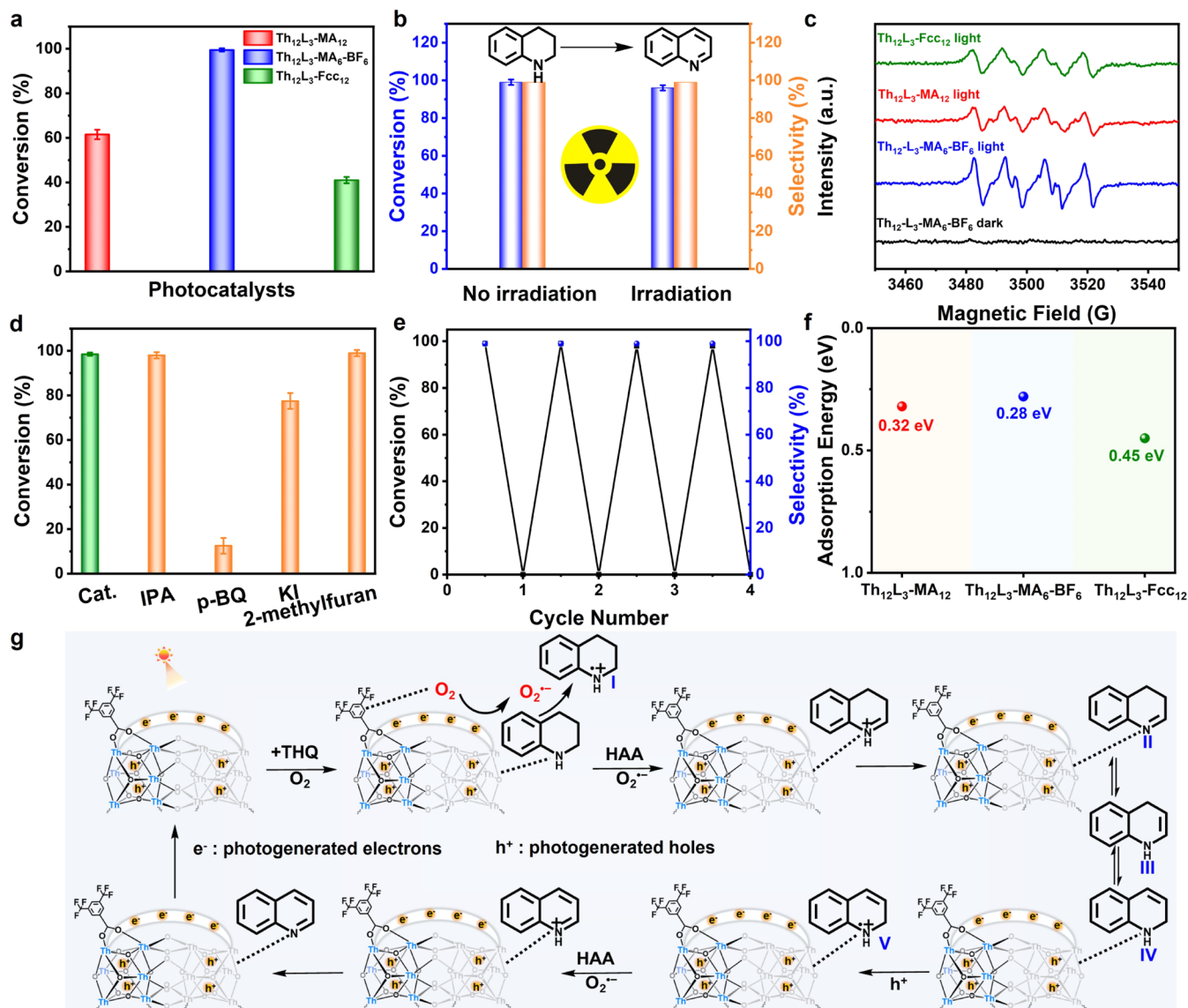


**Figure 4.** Photocatalytic oxo-dehydrogenation of N-heterocycles. (a) Comparison of catalytic properties of three thorium clusters irradiated with  $\gamma$ -rays. (b) Compared catalytic activity of  $\text{Th}_{12}\text{L}_3\text{-MA}_6\text{-BF}_6$  before and after  $\gamma$ -irradiation. (c) EPR spectra of thorium clusters in the presence of DMPO. (d) Some comparative tests added the corresponding sacrificial reagents. (e) The conversion and selectivity of photocatalytic oxo-dehydrogenation of N-heterocycles with  $\text{Th}_{12}\text{L}_3\text{-MA}_6\text{-BF}_6$  in 4 repeating cycles. (f) The calculated adsorption energies of  $\text{O}_2$  on these three thorium clusters. (g) Mechanism for photocatalytic oxo-dehydrogenation of N-heterocycles.

transferred to  $\text{O}_2$ , which is more favorable for the formation of  $\text{O}_2^{\bullet-}$  (Figure S41).<sup>38</sup> Consistently, the distances between the  $\text{O}_2$  adsorption site and LUMO were calculated to be 3.24 (  $\text{Th}_{12}\text{L}_3\text{-MA}_{12}$  ), 2.8 (  $\text{Th}_{12}\text{L}_3\text{-MA}_6\text{-BF}_6$  ), and 3.7 Å (  $\text{Th}_{12}\text{L}_3\text{-Fcc}_{12}$  ). It is clear that  $\text{Th}_{12}\text{L}_3\text{-MA}_6\text{-BF}_6$  has the closest distance, which is more favorable for charge migration. These results suggest that the introduction of 3,5-bis-(trifluoromethyl)benzoic acid significantly promotes  $\text{O}_2$  adsorption and electron transfer, leading to excellent catalytic performance. Based on the aforementioned experimental and theoretical results, a rational catalysis mechanism was propounded (Figure 4g).<sup>39–44</sup> First, 1,2,3,4-THQ is adsorbed in the vicinity of HOMO (probably mainly thorium–oxygen core) and oxidized by photogenerated holes to produce intermediate I. Meanwhile,  $\text{O}_2$  is reduced by photogenerated electrons to produce  $\text{O}_2^{\bullet-}$ . Afterward, intermediate I reacts with  $\text{O}_2^{\bullet-}$  to form intermediate II by sequential hydrogen atom

abstraction (HAA) and deprotonation. Then, intermediate II undergoes an isomerization process to produce intermediates III and IV. At last, the intermediate IV proceeds the second oxidative dehydrogenation process similar to that which 1,2,3,4-THQ endured to form the required product.

**Thermocatalytic Performance toward Oxidation of Diphenylmethane.** The selective oxidation of inert C–H bonds to the respective oxygen-containing compounds has become one of the most vigorous areas of development. As an exemplar of benzylic C–H oxidation, the oxidation of diphenylmethane (DPM) into high-value-added benzophenone has both academic and industrial significance.<sup>45–47</sup> Considering the excellent catalytic performance of thorium clusters in previous reactions as well as their thermal stability, we further extended their thermocatalytic properties. The thorium clusters after  $\gamma$  irradiation were used for the DPM oxidation at 80 °C using TBHP (tertiary-butyl hydroperoxide)



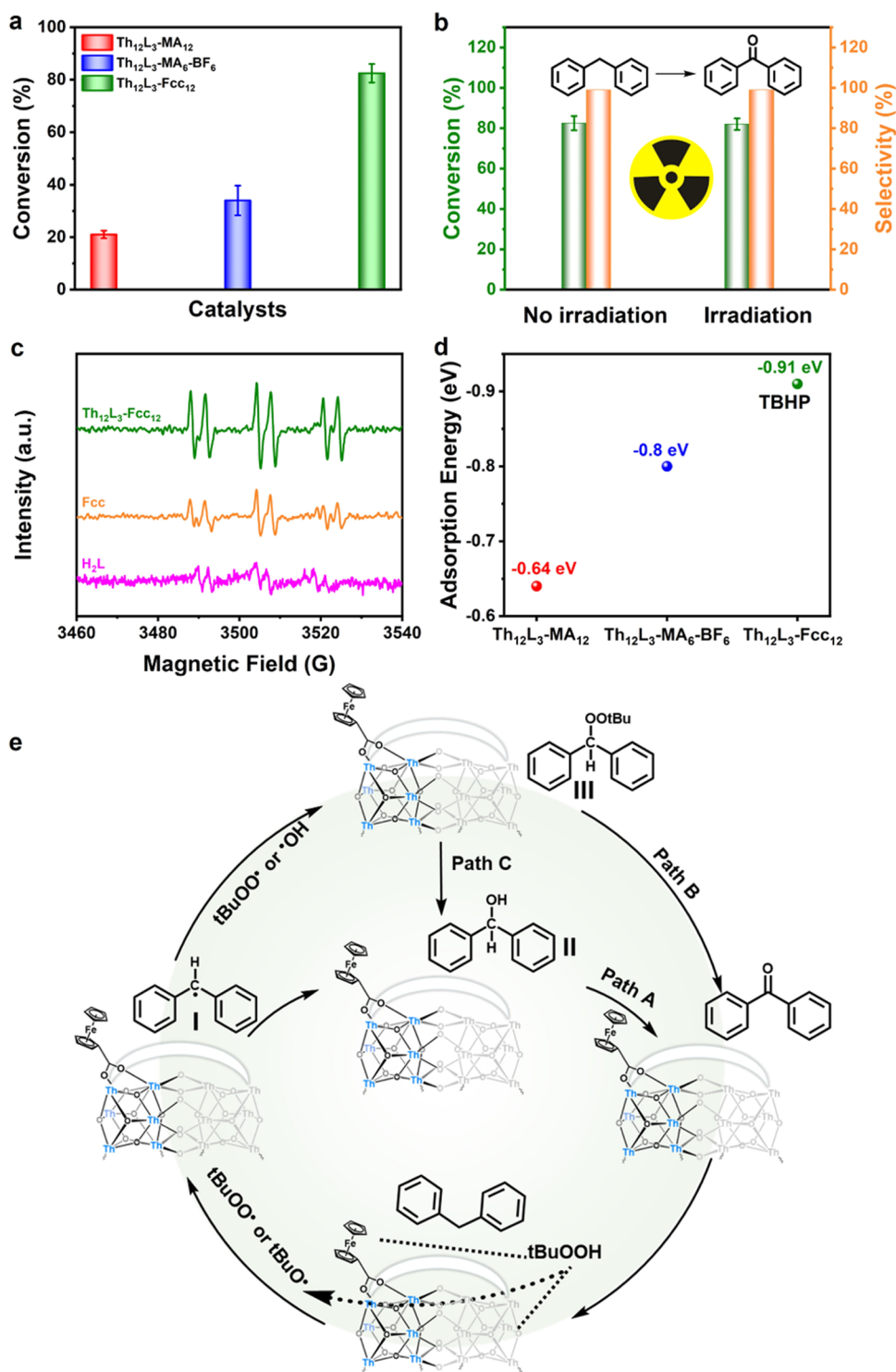


**Figure 5.** Thermocatalytic performance toward the oxidation of diphenylmethane. (a) Comparison of catalytic properties of three thorium clusters irradiated with  $\gamma$ -rays. (b) Compared catalytic activity of  $\text{Th}_{12}\text{L}_3\text{-Fcc}_{12}$  before and after  $\gamma$ -irradiation. (c) EPR spectra of  $\text{Th}_{12}\text{L}_3\text{-Fcc}_{12}$ ,  $\text{H}_2\text{L}$ , and Fcc in the presence of PBN (N-tert-butyl- $\alpha$ -phenylnitron). (d) The calculated adsorption energies of TBHP on these three thorium clusters. (e) Mechanism for thermocatalytic diphenylmethane oxidation.

as the oxidant. As shown in Figure 5a, the conversion of  $\text{Th}_{12}\text{L}_3\text{-Fcc}_{12}$  was significantly higher (84%) compared to  $\text{Th}_{12}\text{L}_3\text{-MA}_{12}$  (20%) and  $\text{Th}_{12}\text{L}_3\text{-MA}_6\text{-BF}_6$  (30%) under the same conditions. It may be due to the fact that the incorporation of Fcc in  $\text{Th}_{12}\text{L}_3\text{-Fcc}_{12}$  enhanced the activation of TBHP. Likewise, the activity of  $\text{Th}_{12}\text{L}_3\text{-Fcc}_{12}$  was similar before and after high-dose  $\gamma$  irradiation (Figure 5b).

Next, a series of controlled experiments were carried out to determine that catalyst and TBHP were essential for the reaction. Similarly to the previous reaction, the catalytic activities of the ligands, metal salts,  $\text{Th}_6$ , and the decomposition products of the thorium clusters were lower than that of  $\text{Th}_{12}\text{L}_3\text{-Fcc}_{12}$ , which reaffirmed the important role of high-nuclear thorium clusters in the catalytic reaction (Tables 1 and

447 S4). In addition, TBHP is generally involved in free-radical  
448 chemistry reactions. Therefore, the oxidation of DPM was  
449 immediately halted when the free-radical scavenger BHT was  
450 added to the reaction mixture (Table S11, entry 4). To further  
451 determine the reactive radicals during the reaction, EPR tests  
452 were carried out at 80 °C in the presence of trapping agent  
453 PBN (N-tert-butyl- $\alpha$ -phenylnitron), which gave clear EPR  
454 peaks for the PBN-spin adducts (Figures S5c and S27).<sup>48,49</sup> The  
455 results indicated that TBHP may generate  $t\text{BuO}^\bullet/t\text{BuOO}^\bullet$   
456 radical during the reaction, which may be the active species of  
457 the reaction. Furthermore, XRD, XPS, and IR results show that  
458  $\text{Th}_{12}\text{L}_3\text{-Fcc}_{12}$  can maintain structural stability under the  
459 reaction conditions (Figures S28–S30). The results of three-  
460 cycle experiments showed that the catalyst was able to  
461 maintain the catalytic activity, and it also displayed excellent  
462 catalytic performance in the oxidation of diphenylmethane  
463 derivatives (Figures S31 and S32).

464 Subsequently, theoretical calculations were carried out to  
465 compare the differences in thermocatalytic properties of these  
466 thorium clusters. Figure S4d shows that among these thorium  
467 clusters,  $\text{Th}_{12}\text{L}_3\text{-Fcc}_{12}$  has the lowest adsorption energy for  
468 TBHP (−0.91 eV), which implies that its activation capacity  
469 for TBHP is stronger, leading to optimal catalytic performance.  
470 In addition, the adsorption energies of TBHP on ligands ( $\text{H}_2\text{L}$   
471 and Fcc) were also calculated (Figure S43). Obviously, the  
472 adsorption energies on the ligands (0.29 eV for  $\text{H}_2\text{L}$  and  
473 −0.034 eV for Fcc) were higher than that of  $\text{Th}_{12}\text{L}_3\text{-Fcc}_{12}$   
474 (−0.91 eV), which suggested that the catalytic activity of the  
475 ligands alone is poor (Table 1). Therefore, on  $\text{Th}_{12}\text{L}_3\text{-Fcc}_{12}$ ,  
476 there should be a synergistic activation of TBHP by thorium-  
477 oxo core and ligands. These calculations are also in agreement  
478 with the EPR test results (Figure S5c). The mechanism for the  
479 oxidation of DPM catalyzed by the  $\text{Th}_{12}\text{L}_3\text{-Fcc}_{12}$  was proposed  
480 based on the above results and previous report (Figure  
481 S5e).<sup>50,51</sup> TBHP is adsorbed and activated on the thorium-oxo  
482 core and the Fcc ligand to generate  $t\text{BuO}^\bullet/t\text{BuOO}^\bullet$  radical.  
483 Subsequently, these radicals extract one H atoms of DPM to  
484 produce intermediate I, which can either react with  $^\bullet\text{OH}$  or  
485  $t\text{BuOO}^\bullet$  to form the oxygenated intermediate II or III.  
486 Intermediate II can be further oxidized to form the target  
487 product (path A), while intermediate III can remove one  
488 molecule of  $t\text{BuOH}$  to form ketone directly (path B), or it can  
489 be converted to intermediate II to obtain the target product  
490 (path C and path A).

## 491 ■ CONCLUSIONS

492 In summary, we have designed and synthesized for the first  
493 time under mild conditions a series of novel high-nuclear  
494 thorium clusters with similar core structures, which were  
495 subjected to irradiation by 690 kGy  $\gamma$ -rays without significant  
496 changes in their molecular structures and compositions.  
497 Therefore, we investigated the catalytic activity of these  
498 functionalized irradiation-resistant thorium clusters for the first  
499 time. It was found that their catalytic activity was comparable  
500 to that before  $\gamma$ -ray irradiation, which implies that these  
501 thorium clusters will be expected to be used for catalysis under  
502 ionizing radiation conditions in the future when they are  
503 warranted. In addition, the ligand engineering has extended the  
504 range of catalytic applications of thorium clusters, such as  
505 reduction reactions (photocatalytic nitroarene reduction) and  
506 some oxidation reactions (photocatalytic N-heterocyclic  
507 oxidative dehydrogenation and thermocatalytic diphenyl-  
508 methane oxidation). Product selectivity of >99% and

conversion of >80% were achieved in all of the photo/ 509  
thermocatalytic reactions. Subsequent irradiation experiments 510  
as well as DFT calculations demonstrated that in these thorium 511  
clusters, synergistic activation between ligands and thorium- 512  
oxo core leads to the production of specific active species ( $\text{H}^+$ , 513  
 $\text{O}_2^{\bullet-}$  or  $t\text{BuO}^\bullet/t\text{BuOO}^\bullet$ ), thereby enhancing catalytic 514  
performance. This work provides new and exemplary research 515  
for the synthesis of highly nucleated thorium clusters as well as 516  
for the development of broader photo/thermal catalytic 517  
properties of radiation-stabilized thorium clusters. 518

## 519 ■ ASSOCIATED CONTENT

### 520 ⓘ Supporting Information

The Supporting Information is available free of charge at 521  
<https://pubs.acs.org/doi/10.1021/jacs.4c03126>. 522

Detailed information regarding the experimental meth- 523  
ods, characterization analysis, DFT calculations (PDF) 524

### 525 Accession Codes

CCDC 2257702, 2257745, and 2286776 contain the 526  
supplementary crystallographic data for this paper. These 527  
data can be obtained free of charge via [www.ccdc.cam.ac.uk/](http://www.ccdc.cam.ac.uk/data_request/cif) 528  
[data\\_request/cif](http://www.ccdc.cam.ac.uk/data_request/cif), or by emailing [data\\_request@ccdc.cam.ac](mailto:data_request@ccdc.cam.ac.uk). 529  
[uk](mailto:data_request@ccdc.cam.ac.uk), or by contacting The Cambridge Crystallographic Data 530  
Centre, 12 Union Road, Cambridge CB2 1EZ, UK; fax: +44 531  
1223 336033. 532

## 533 ■ AUTHOR INFORMATION

### 534 Corresponding Authors

Jiang Liu — Guangdong Provincial Key Laboratory of Carbon 535  
Dioxide Resource Utilization, School of Chemistry, South 536  
China Normal University, Guangzhou 510006, P. R. China; 537  
[orcid.org/0000-0002-2596-4928](https://orcid.org/0000-0002-2596-4928); Email: [liuj0828@](mailto:liuj0828@m.scnu.edu.cn) 538  
[m.scnu.edu.cn](mailto:m.scnu.edu.cn), [liuj@njnu.edu.cn](mailto:liuj@njnu.edu.cn) 539

Ya-Qian Lan — Jiangsu Collaborative Innovation Centre of 540  
Biomedical Functional Materials, Jiangsu Key Laboratory of 541  
New Power Batteries, School of Chemistry and Materials 542  
Science, Nanjing Normal University, Nanjing 210023, P. R. 543  
China; Guangdong Provincial Key Laboratory of Carbon 544  
Dioxide Resource Utilization, School of Chemistry, South 545  
China Normal University, Guangzhou 510006, P. R. China; 546  
[orcid.org/0000-0002-2140-7980](https://orcid.org/0000-0002-2140-7980); Email: [yqlan@](mailto:yqlan@m.scnu.edu.cn) 547  
[m.scnu.edu.cn](mailto:m.scnu.edu.cn), [yqlan@njnu.edu.cn](mailto:yqlan@njnu.edu.cn); [http://](http://www.yqlangroup.com) 548  
[www.yqlangroup.com](http://www.yqlangroup.com) 549

### 550 Authors

Qian Niu — Jiangsu Collaborative Innovation Centre of 551  
Biomedical Functional Materials, Jiangsu Key Laboratory of 552  
New Power Batteries, School of Chemistry and Materials 553  
Science, Nanjing Normal University, Nanjing 210023, P. R. 554  
China 555

Tao-Yuan Yu — Jiangsu Collaborative Innovation Centre of 556  
Biomedical Functional Materials, Jiangsu Key Laboratory of 557  
New Power Batteries, School of Chemistry and Materials 558  
Science, Nanjing Normal University, Nanjing 210023, P. R. 559  
China 560

Jing-Wen Shi — Guangdong Provincial Key Laboratory of 561  
Carbon Dioxide Resource Utilization, School of Chemistry, 562  
South China Normal University, Guangzhou 510006, P. R. 563  
China 564

Qing Huang — College of Materials Science and Engineering, 565  
Nanjing Forestry University, Nanjing 210037, P. R. China 566

567 **Long-Zhang Dong** – Guangdong Provincial Key Laboratory  
568 of Carbon Dioxide Resource Utilization, School of Chemistry,  
569 South China Normal University, Guangzhou 510006, P. R.  
570 China; [orcid.org/0000-0002-9276-5101](https://orcid.org/0000-0002-9276-5101)  
571 **Fei Yu** – Jiangsu Collaborative Innovation Centre of  
572 Biomedical Functional Materials, Jiangsu Key Laboratory of  
573 New Power Batteries, School of Chemistry and Materials  
574 Science, Nanjing Normal University, Nanjing 210023, P. R.  
575 China; [orcid.org/0000-0001-9721-271X](https://orcid.org/0000-0001-9721-271X)  
576 **Shun-Li Li** – Guangdong Provincial Key Laboratory of  
577 Carbon Dioxide Resource Utilization, School of Chemistry,  
578 South China Normal University, Guangzhou 510006, P. R.  
579 China

580 Complete contact information is available at:  
581 <https://pubs.acs.org/10.1021/jacs.4c03126>

## 582 Author Contributions

583 <sup>||</sup>Q.N. and T.-Y.Y. contributed equally to this work. All of the  
584 authors reviewed and contributed to this paper.

## 585 Notes

586 The authors declare no competing financial interest.

## 587 ■ ACKNOWLEDGMENTS

588 This study was financially supported by the National Key R&D  
589 Program of China (2023YFA1507204 and 2023YFA1507201),  
590 the NSFC (Nos. 22225109, 22271104, 21871141, 21871142,  
591 22101089, 22071109, and 22301139), the Top Youth Project  
592 of Guangdong Province Pearl River Talents Program  
593 (2021QNo2L617), the Excellent Youth Foundation of Jiangsu  
594 Natural Science Foundation (No. BK20211593), the Natural  
595 Science Foundation of Jiangsu Province (Grant No. BK  
596 20230375), and the Postgraduate Research and Practice  
597 Innovation Program of Jiangsu Province (KYCX23\_1685).

## 598 ■ REFERENCES

599 (1) Knope, K. E.; Vasiliev, M.; Dixon, D. A.; Soderholm, L.  
600 Thorium(IV)-selenate clusters containing an octanuclear Th(IV)  
601 hydroxide/oxide core. *Inorg. Chem.* **2012**, *51* (7), 4239–4249.  
602 (2) Wang, Y.; Liu, W.; Bai, Z.; Zheng, T.; Silver, M. A.; Li, Y.; Wang,  
603 Y.; Wang, X.; Diwu, J.; Chai, Z.; Wang, S. Employing an Unsaturated  
604 Th(IV) Site in a Porous Thorium-Organic Framework for Kr/Xe  
605 Uptake and Separation. *Angew. Chem., Int. Ed.* **2018**, *57* (20), 5783–  
606 5787.  
607 (3) Lu, H.; Xu, M.; Zheng, Z.; Liu, Q.; Qian, J.; Zhang, Z. H.; He,  
608 M. Y.; Qian, Y.; Wang, J. Q.; Lin, J. Emergence of Thorium-Based  
609 Polyoxo Clusters as a Platform for Selective X-ray Dosimetry. *Inorg.*  
610 *Chem.* **2021**, *60* (24), 18629–18633.  
611 (4) Ejegbavwo, O. A.; Martin, C. R.; Olorunfemi, O. A.; Leith, G. A.;  
612 Ly, R. T.; Rice, A. M.; Dolgoplova, E. A.; Smith, M. D.; Karakalos, S.  
613 G.; Birkner, N.; Powell, B. A.; Pandey, S.; Koch, R. J.; Mixture, S. T.;  
614 Loye, H. Z.; Phillpot, S. R.; Brinkman, K. S.; Shustova, N. B.  
615 Thermodynamics and Electronic Properties of Heterometallic Multi-  
616 nuclear Actinide-Containing Metal-Organic Frameworks with "Struc-  
617 tural Memory". *J. Am. Chem. Soc.* **2019**, *141* (29), 11628–11640.  
618 (5) Lv, K.; Fichter, S.; Gu, M.; März, J.; Schmidt, M. An updated  
619 status and trends in actinide metal-organic frameworks (An-MOFs):  
620 From synthesis to application. *Coord. Chem. Rev.* **2021**, *446* (1),  
621 No. 214011.  
622 (6) Karmel, I. S. R.; Tamm, M.; Eisen, M. S. Actinide-Mediated  
623 Catalytic Addition of E-H Bonds (E = N, P, S) to Carbodiimides,  
624 Isocyanates, and Isothiocyanates. *Angew. Chem., Int. Ed.* **2015**, *54*  
625 (42), 12422–12425.  
626 (7) Liu, H.; Eisen, M. S. Selective Actinide-Catalyzed Tandem  
627 Proton-Transfer Esterification of Aldehydes with Alcohols for the

Production of Asymmetric Esters. *Organometallics* **2017**, *36* (8), 628  
1461–1464. 629  
(8) Makarov, K.; Ritacco, I.; Fridman, N.; Caporaso, L.; Eisen, M. S. 630  
Against All Odds, Uranium and Thorium Iminato Complexes Enable 631  
the Cleavage of C = O Bonds in Isocyanates. *ACS Catal.* **2023**, *13* 632  
(17), 11798–11814. 633  
(9) Li, X. F.; Wu, P.; Kan, L.; Niu, Q.; Sun, S. N.; Huang, Q.; Lan, Y. 634  
Q. Integrating Metal Complex Units and Redox Sites into Thorium- 635  
Based Metal–Organic Frameworks for Selective Photocatalytic 636  
Oxidation of Sulfides. *Adv. Funct. Mater.* **2023**, *33*, No. 2308534. 637  
(10) Ghatak, T.; Drucker, S.; Fridman, N.; Eisen, M. S. Thorium 638  
complexes possessing expanded ring N-heterocyclic iminato ligands: 639  
synthesis and applications. *Dalton Trans.* **2017**, *46* (36), 12005– 640  
12009. 641  
(11) Ghatak, T.; Makarov, K.; Fridman, N.; Eisen, M. S. Catalytic 642  
regeneration of a Th–H bond from a Th–O bond through a mild and 643  
chemoselective carbonyl hydroboration. *Chem. Commun.* **2018**, *54* 644  
(78), 11001–11004. 645  
(12) Saha, S.; Eisen, M. S. Mild catalytic deoxygenation of amides 646  
promoted by thorium metallocene. *Dalton Trans.* **2020**, *49* (36), 647  
12835–12841. 648  
(13) Tian, X. R.; Jiang, Z. Y.; Hou, S. L.; Hu, H. S.; Li, J.; Zhao, B. A. 649  
Strong-Acid-Resistant [Th<sub>6</sub>] Cluster-Based Framework for Effectively 650  
and Size-Selectively Catalyzing Reductive Amination of Aldehydes 651  
with N,N-Dimethylformamide. *Angew. Chem., Int. Ed.* **2023**, 652  
No. e202301764. 653  
(14) Qian, X. Y.; Zhou, T. H.; Mao, J. G. New thorium(IV)-arsonates 654  
with a [Th<sub>8</sub>O<sub>13</sub>]<sup>6+</sup> octanuclear core. *Dalton Trans.* **2015**, *44* (30), 655  
13573–13580. 656  
(15) Chen, R.; Qin, G.; Li, S.; Edwards, A. J.; Piltz, R. O.; Del Rosal, 657  
I.; Maron, L.; Cui, D.; Cheng, J. Molecular Thorium Trihydrido 658  
Clusters Stabilized by Cyclopentadienyl Ligands. *Angew. Chem., Int.* 659  
*Ed.* **2020**, *59* (28), 11250–11255. 660  
(16) Woody, P.; Kraus, F. [Th<sub>10</sub>(μ-F<sub>16</sub>)(μ<sub>3</sub>-O<sub>4</sub>)(μ<sub>4</sub>-O<sub>4</sub>)(NH<sub>3</sub>)<sub>32</sub>]- 661  
(NO<sub>3</sub>)<sub>8</sub>·19.6 NH<sub>3</sub>·the Largest Thorium Complex from Solution 662  
known to Date. *Z. Anorg. Allg. Chem.* **2014**, *640* (8–9), 1547–1550. 663  
(17) Kong, X. H.; Wu, Q. Y.; Mei, L.; Zeng, L. W.; Huang, Z. W.; 664  
Yu, J. P.; Nie, C. M.; Gibson, J. K.; Chai, Z. F.; Hu, K. Q.; Shi, W. Q. 665  
Silver Ion-Induced Formation of Unprecedented Thorium Nonamer 666  
Clusters via Lacuna-Construction Strategy. *CCS Chem.* **2022**, *5* (5), 667  
1144–1153. 668  
(18) Tutson, C. D.; Gorden, A. E. V. Thorium coordination: A 669  
comprehensive review based on coordination number. *Coord. Chem.* 670  
*Rev.* **2017**, *333*, 27–43. 671  
(19) Li, P.; Wang, X.; Otake, K.-i.; Lyu, J.; Hanna, S. L.; Islamoglu, 672  
T.; Farha, O. K. Synthetic Control of Thorium Polyoxo-Clusters in 673  
Metal-Organic Frameworks toward New Thorium-Based Materials. 674  
*ACS Appl. Nano Mater.* **2019**, *2* (4), 2260–2265. 675  
(20) Zanonato, P. L.; Di Bernardo, P.; Zhang, Z.; Gong, Y.; Tian, G.; 676  
Gibson, J. K.; Rao, L. Hydrolysis of thorium(IV) at variable 677  
temperatures. *Dalton Trans.* **2016**, *45* (32), 12763–12771. 678  
(21) Li, Z. J.; Guo, X.; Qiu, J.; Lu, H.; Wang, J. Q.; Lin, J. Recent 679  
advances in the applications of thorium-based metal-organic frame- 680  
works and molecular clusters. *Dalton Trans.* **2022**, *51* (19), 7376– 681  
7389. 682  
(22) Hou, S.; Liu, F.; Xie, H.; Hanna, S. L.; Idrees, K. B.; Zhang, C.; 683  
Wang, X.; Chen, Y.; Li, P.; Farha, O. K. Unveiling the Structure- 684  
Modulator Relationships in Thorium-Based Metal-Organic Frame- 685  
work Crystallization. *Inorg. Chem.* **2023**, *62* (14), 5479–5486. 686  
(23) Ju, Y.; Li, Z. J.; Lu, H.; Zhou, Z.; Li, Y.; Wu, X. L.; Guo, X.; 687  
Qian, Y.; Zhang, Z. H.; Lin, J.; Wang, J. Q.; He, M. Y. 688  
Interpenetration Control in Thorium Metal-Organic Frameworks: 689  
Structural Complexity toward Iodine Adsorption. *Inorg. Chem.* **2021**, 690  
*60* (8), 5617–5626. 691  
(24) Niu, Q.; Huang, Q.; Yu, T.-Y.; Liu, J.; Shi, J.-W.; Dong, L.-Z.; 692  
Li, S.-L.; Lan, Y.-Q. Achieving High Photo/Thermocatalytic Product 693  
Selectivity and Conversion via Thorium Clusters with Switchable 694  
Functional Ligands. *J. Am. Chem. Soc.* **2022**, *144* (40), 18586–18594. 695



- (25) Lu, H.; Xie, J.; Wang, X. Y.; Wang, Y.; Li, Z. J.; Diefenbach, K.; Pan, Q. J.; Qian, Y.; Wang, J. Q.; Wang, S.; Lin, J. Visible colorimetric dosimetry of UV and ionizing radiations by a dual-module photochromic nanocluster. *Nat. Commun.* **2021**, *12* (1), No. 2798.
- (26) Gilson, S. E.; Fairley, M.; Julien, P.; Oliver, A. G.; Hanna, S. L.; Arntz, G.; Farha, O. K.; LaVerne, J. A.; Burns, P. C. Unprecedented Radiation Resistant Thorium-Binaphthol Metal-Organic Framework. *J. Am. Chem. Soc.* **2020**, *142* (31), 13299–13304.
- (27) Lu, H.; Hou, H.; Hou, Y. C.; Zheng, Z.; Ma, Y.; Zhou, Z.; Guo, X.; Pan, Q. J.; Wang, Y.; Qian, Y.; Wang, J. Q.; Lin, J. A New Concept of Radiation Detection Based on a Fluorochromic and Piezochromic Nanocluster. *J. Am. Chem. Soc.* **2022**, *144* (8), 3449–3457.
- (28) Zheng, Z.; Lu, H.; Hou, H.; Bai, Y.; Qiu, J.; Guo, X.; Wang, J. Q.; Lin, J. Stepwise Crystallization of Millimeter Scale Thorium Cluster Single Crystals as a Bifunctional Platform for X-ray Detection and Shielding. *Small* **2023**, *19* (10), No. e2206782.
- (29) Luo, Z. R.; Wang, H. L.; Zhu, Z. H.; Liu, T.; Ma, X. F.; Wang, H. F.; Zou, H. H.; Liang, F. P. Assembly of Dy(60) and Dy(30) cage-shaped nanoclusters. *Commun. Chem.* **2020**, *3* (1), No. 30.
- (30) Li, Y. L.; Wang, H. L.; Zhu, Z. H.; Liang, F. P.; Zou, H. H. Giant Crown-Shaped Dy(34) Nanocluster with High Acid-Base Stability Assembled by an out-to-in Growth Mechanism. *Inorg. Chem.* **2022**, *61* (26), 10101–10107.
- (31) Anuchai, S.; Juntrapirom, S.; Jarusupakornkul, K.; Tantraviwat, D.; Inceesungvorn, B. Oxygen vacancy-rich BiOBr microflowers for enhancing photocatalytic reduction of nitrobenzene under visible light. *Colloids Surf., A* **2023**, *664*, No. 131102, DOI: 10.1016/j.colsurfa.2023.131102.
- (32) Phasayavan, W.; Boochakiat, S.; Pluengphon, P.; Tantraviwat, D.; Inceesungvorn, B. Tuning product selectivity in nitrobenzene reduction over a single Bi<sub>2</sub>MoO<sub>6</sub> photocatalyst in one pot: Mechanisms and roles of reaction compositions. *J. Photochem.* **2022**, *432*, No. 114099, DOI: 10.1016/j.jphotochem.2022.114099.
- (33) Cheruvathoor Poulouse, A.; Zoppellaro, G.; Konidakis, I.; Serpetzoglou, E.; Stratakis, E.; Tomanec, O.; Beller, M.; Bakandritsos, J.; Zboril, R. Fast and selective reduction of nitroarenes under visible light with an earth-abundant plasmonic photocatalyst. *Nat. Nanotechnol.* **2022**, *17* (5), 485–492.
- (34) Jiao, J.; Sun, H.; Si, C.; Xu, J.; Zhang, T.; Han, Q. Photocatalytic Multielectron Reduction of Nitroarenes to Anilines by Utilizing an Electron-Storable Polyoxometalate-Based Metal-Organic Framework. *ACS Appl. Mater. Interfaces* **2022**, *14* (14), 16386–16393.
- (35) Balayeva, N. O.; Mamiyev, Z.; Dillert, R.; Zheng, N.; Bahnemann, D. W. Rh/TiO<sub>2</sub>-Photocatalyzed Acceptorless Dehydrogenation of N-Heterocycles upon Visible-Light Illumination. *ACS Catal.* **2020**, *10* (10), 5542–5553.
- (36) Zheng, M.; Shi, J.; Yuan, T.; Wang, X. Metal-Free Dehydrogenation of N-Heterocycles by Ternary h-BCN Nanosheets with Visible Light. *Angew. Chem., Int. Ed.* **2018**, *57* (19), 5487–5491.
- (37) Gong, X.; Shu, Y.; Jiang, Z.; Lu, L.; Xu, X.; Wang, C.; Deng, H. Metal-Organic Frameworks for the Exploitation of Distance between Active Sites in Efficient Photocatalysis. *Angew. Chem., Int. Ed.* **2020**, *59* (13), 5326–5331.
- (38) Li, S.; Yin, J.; Zhang, H.; Zhang, K. A. I. Dual Molecular Oxygen Activation Sites on Conjugated Microporous Polymers for Enhanced Photocatalytic Formation of Benzothiazoles. *ACS Appl. Mater. Interfaces* **2023**, *15* (2), 2825–2831.
- (39) Zhang, Z.; Liu, W.; Zhang, Y.; Bai, J.; Liu, J. Bioinspired Atomic Manganese Site Accelerates Oxo-Dehydrogenation of N-Heterocycles over a Conjugated Tri-s-Triazine Framework. *ACS Catal.* **2021**, *11* (1), 313–322.
- (40) Balayeva, N. O.; Zheng, N.; Dillert, R.; Bahnemann, D. W. Visible-Light-Mediated Photocatalytic Aerobic Dehydrogenation of N-heterocycles by Surface-Grafted TiO<sub>2</sub> and 4-amino-TEMPO. *ACS Catal.* **2019**, *9* (12), 10694–10704.
- (41) Chen, S.; Wan, Q.; Badu-Tawiah, A. K. Picomole-Scale Real-Time Photoreaction Screening: Discovery of the Visible-Light-Promoted Dehydrogenation of Tetrahydroquinolines under Ambient Conditions. *Angew. Chem., Int. Ed.* **2016**, *55* (32), 9345–9349.
- (42) Wendlandt, A. E.; Stahl, S. S. Modular o-quinone catalyst system for dehydrogenation of tetrahydroquinolines under ambient conditions. *J. Am. Chem. Soc.* **2014**, *136* (34), 11910–11913.
- (43) Lu, Y. L.; Song, J. Q.; Qin, Y. H.; Guo, J.; Huang, Y. H.; Zhang, X. D.; Pan, M.; Su, C. Y. A Redox-Active Supramolecular Fe(4)L(6) Cage Based on Organic Vertices with Acid-Base-Dependent Charge Tunability for Dehydrogenation Catalysis. *J. Am. Chem. Soc.* **2022**, *144* (19), 8778–8788.
- (44) Zhang, Y.; Song, T.; Zhou, X.; Yang, Y. Oxygen-vacancy-boosted visible light driven photocatalytic oxidative dehydrogenation of saturated N-heterocycles over Nb<sub>2</sub>O<sub>5</sub> nanorods. *Appl. Catal., B* **2022**, *316*, No. 121622, DOI: 10.1016/j.apcatb.2022.121622.
- (45) Garcia-Bosch, I.; Siegler, M. A. Copper-Catalyzed Oxidation of Alkanes with H<sub>2</sub>O<sub>2</sub> under a Fenton-like Regime. *Angew. Chem., Int. Ed.* **2016**, *55* (41), 12873–12876.
- (46) Wang, X.; Liu, M.; Wang, Y.; Fan, H.; Wu, J.; Huang, C.; Hou, H. Cu(I) Coordination Polymers as the Green Heterogeneous Catalysts for Direct C-H Bonds Activation of Arylalkanes to Ketones in Water with Spatial Confinement Effect. *Inorg. Chem.* **2017**, *56* (21), 13329–13336.
- (47) Guo, C.; Zhang, Y.; Zhang, Y.; Wang, J. An efficient approach for enhancing the catalytic activity of Ni-MOF-74 via a relay catalyst system for the selective oxidation of benzylic C-H bonds under mild conditions. *Chem. Commun.* **2018**, *54* (30), 3701–3704.
- (48) Daliran, S.; Santiago-Portillo, A.; Navalon, S.; Oveisi, A. R.; Alvaro, M.; Ghorbani-Vaghei, R.; Azarifar, D.; Garcia, H. Cu(II)-Schiff base covalently anchored to MIL-125(Ti)-NH(2) as heterogeneous catalyst for oxidation reactions. *J. Colloid Interface Sci.* **2018**, *532*, 700–710.
- (49) Kimberley, L.; Sheveleva, A. M.; Li, J.; Carter, J. H.; Kang, X.; Smith, G. L.; Han, X.; Day, S. J.; Tang, C. C.; Tuna, F.; McInnes, E. J. L.; Yang, S.; Schroder, M. The Origin of Catalytic Benzylic C-H Oxidation over a Redox-Active Metal-Organic Framework. *Angew. Chem., Int. Ed.* **2021**, *60* (28), 15243–15247.
- (50) Ju, Z. Y.; Song, L. N.; Chong, M. B.; Cheng, D. G.; Hou, Y.; Zhang, X. M.; Zhang, Q. H.; Ren, L. H. Selective Aerobic Oxidation of C(sp<sup>3</sup>)-H Bonds Catalyzed by Yeast-Derived Nitrogen, Phosphorus, and Oxygen Codoped Carbon Materials. *J. Org. Chem.* **2022**, *87* (6), 3978–3988.
- (51) Tan, J.; Zheng, T.; Yu, Y.; Xu, K. TBHP-promoted direct oxidation reaction of benzylic Csp<sup>3</sup>-H bonds to ketones. *RSC Adv.* **2017**, *7* (25), 15176–15180.